

## A simplified model for understanding natural convection driven biomass cooking stoves—Part 2: With cook piece operation and the dimensionless form

Joshua Agenbrood<sup>\*</sup>, Morgan DeFoort, Allan Kirkpatrick, Cory Kreutzer

Engines and Energy Conversion Laboratory, Department of Mechanical Engineering, Colorado State University, 430 N. College Ave. Fort Collins, Colorado (80821), USA

### ARTICLE INFO

#### Article history:

Received 30 September 2010

Revised 2 April 2011

Accepted 2 April 2011

Available online 4 May 2011

#### Keywords:

Cook stove

Chimney effect

Analytical model

Design

Emissions

Efficiency

### ABSTRACT

In the preceding work of Part 1: Setup and Baseline Validation, a simple model was developed for understanding the simplified, but fundamental operating behavior of natural convection biomass cooking stoves. The model predicts combustion chamber bulk flow parameters—including mass flow rate, temperature, and excess air ratio—from stove design and operation inputs such as geometry and firepower. In the following work of Part 2, this model will be developed further into a dimensionless form. The dimensionless solution reveals generalized natural convection stove behavior common to all such stoves. The experimental implementation of the dimensionless form provides a reduction of independent parameters, and allows for the bulk flow rate, temperature, and even emissions from various stove configurations to be plotted together, for direct comparison, with a single trend for each parameter. Model validation presented in Part 1 is for stove operation without a cook piece in place; in Part 2, model validation is extended to more practical, with cook piece, stove operation. An increased loss coefficient is experimentally determined to account for the added cook piece restriction; with the new coefficient, the model is shown to remain both applicable and accurate. As in Part 1, carbon monoxide and particulate matter emissions are recorded in conjunction with model validation. With the cook piece now in place, an upper limit to both firepower and efficient combustion will be observed. Applying the dimensionless firepower axis to the emission data from this, and the preceding work, trends for both carbon monoxide and particulate matter form a single trend for three stove configurations. With the consolidated data, the two emission criteria trend together, and a region of improved emissions is observed over a medium dimensionless firepower range.

© 2011 International Energy Initiative. Published by Elsevier Inc. All rights reserved.

### Introduction

As introduced in the proceeding work of Part 1, Agenbrood et al. (2011), improved biomass cooking stoves have the potential to impact indoor air quality, deforestation, climate change, and quality of life on a global scale. The majority of these improved cooking stoves operate in a natural convection mode. The design of these stoves can significantly impact their performance and to what extent their emissions and efficiency can be considered improved. Although these improved biomass stoves have been of interest for several decades, a theoretical understanding of their operating behavior and the development of engineering tools for their design are notably lacking.

In Part 1, Agenbrood et al. (2011), a model was developed for understanding the simplified, but fundamental operating behavior of these natural convection biomass cooking stoves. The model predicts combustion chamber bulk flow rate, temperature, and excess air ratio from stove design and operation inputs.

The model developed utilized the dimensional form of a two equation system. In the following work, the model system will be further

developed into a dimensionless form. With the dimensionless form we observe the fundamental, generalized operating behavior common to all natural convection cooking stoves. The dimensionless form also provides a reduction of experimentally independent parameters, allowing bulk flow rate, temperature, and even emission data from various stove configurations (geometry, cook piece, etc.) to be analyzed with a single trend for each parameter. This feature is shown to be particularly interesting when plotting stove emissions.

Part 1, Agenbrood et al. (2011) validation results were presented for cooking stove operation similar to actual stove use with the exception that a cook piece (pot) was not in place. The without cook piece configuration was useful for isolating basic model physics and assessing baseline model accuracy while minimizing the effect of the unknown loss coefficient and neglected heat transfer. However, operation without a cook piece in place is inherently not useful for actual cooking use. In this work validation, analogous to that of the preceding work, will be presented for the more practical case of operation with the cook piece now in place. A new loss coefficient, accounting for the increased restriction resulting from the cook piece obstruction, will be experimentally determined. With the new loss coefficient the simplified stove flow model will remain both applicable and accurate for stove operation with the cook piece in place.

The dimensionless form will be applied to the experimental validation results from the three stove configurations utilized thus far—two stove

<sup>\*</sup> Corresponding author. Tel.: +1 970 491 4796.

E-mail address: [jagenbro@gmail.com](mailto:jagenbro@gmail.com) (J. Agenbrood).

geometries from the preceding work and the with cook piece configuration of this work. The dimensionless form will be shown to allow direct comparison of the validation results from the three configurations using a single bulk mass flow rate and temperature trend for each parameter.

Carbon monoxide (CO) and particulate matter (PM) emission data will once again be recorded in conjunction with validation data. Low firepower, high excess air ratio emissions behavior will be consistent with the proceeding work. The high firepower, low excess air ratio limit to efficient combustion proposed, although not encountered, in the previous work will now be observed with the cook piece in place.

The dimensionless firepower axis can also be applied to the emission data, and will be shown to provide a particularly useful reduction of independent experimental parameters. With the dimensionless axis, CO and PM emission data from the three stove configurations will be plotted using a single trend for each emission criteria. CO and PM emissions are observed to be consistent between the three stove configurations, and also to trend together. With the consolidated CO and PM data from the three stove configurations, a region of improved emissions will be observed over a medium dimensionless firepower range.

With these interesting results, overall model conclusions are discussed, and the case is made for further research.

### Development of the dimensionless system

The two equation system for stove flow introduced and validated in Agenbrood et al. (2011) can be further developed into a dimensionless form. Advantages of working in this dimensionless form include scale similarity and reducing the number of independent parameters for experimentation. In the case of the model presented here, the dimensionless form offers an additional advantage. Solving the dimensionless system of equations to be developed, dimensionless stove behavior is plotted and is independent of stove geometry. The resulting plots can be used as a reference to lookup and calculate solutions without solving the system of equations (in this case iteratively).

The two equation system defining the simplified stove model developed in Agenbrood et al. (2011) are repeated below in Eq. (1) and Eq. (2). The equations represent the chimney effect and heat addition processes.

$$\dot{m}_A = CA \left( \frac{P}{RT_H} \right) \cdot \sqrt{2gh \left( \frac{T_H - T_{Amb}}{T_{Amb}} \right)} \quad (1)$$

$$\dot{Q}_{in} = \dot{m}_A c_p (T_H - T_{Amb}) \quad (2)$$

### Dimensionless chimney effect equation

The dimensionless temperature group shown in Eq. (3) can be formed immediately by inspection. This group is fairly common, particularly when working with heat transfer or combustion.

$$T^* \equiv \frac{T_H - T_{Amb}}{T_{Amb}} \quad (3)$$

Substituting Eq. (3) into Eq. (1) and rearranging yields Eq. (4).

$$\begin{aligned} \dot{m}_A &= CA \left( \frac{P}{RT_{Amb}(T^* + 1)} \right) \sqrt{2ghT^*} \\ &= CA \left( \frac{P}{RT_{Amb}} \right) \left( \frac{\sqrt{2ghT^*}}{T^* + 1} \right) \end{aligned} \quad (4)$$

Recognizing  $(P/RT_{Amb})$  as the ambient density ( $\rho_{Amb}$ ), substituting, and rearranging as shown in Eq. (5), the dimensionless mass flow rate group can be defined as shown in Eq. (6). This dimensionless mass flow rate can be understood as the ratio of the actual mass flow rate to the “characteristic natural convection mass flow rate for the given geometry”.

$$\frac{\dot{m}_A}{CA\rho_{Amb}\sqrt{gh}} = \frac{\sqrt{2T^*}}{T^* + 1} \quad (5)$$

$$\dot{m}_A^* \equiv \frac{\dot{m}_A}{CA\rho_{Amb}\sqrt{gh}} \quad (6)$$

Using the dimensionless mass flow rate  $\dot{m}_A^*$  of Eq. (6), the final form of the dimensionless chimney effect equation becomes that of Eq. (7).

$$\dot{m}_A^* = \frac{\sqrt{2T^*}}{T^* + 1} \quad (7)$$

### Dimensionless heat addition equation

For the dimensionless heat addition equation it becomes convenient to use a mass burn rate of fuel instead of the firepower as used in Agenbrood et al. (2011); the two are related as shown in Eq. (8).

$$\dot{Q}_{in} = \dot{m}_F HV \quad (8)$$

Substituting Eq. (8) and Eq. (3) into Eq. (2) and rearranging into Eq. (9), a dimensionless heating value group,  $(HV^*)$ , is formed as defined in Eq. (10). This group can be understood as the ratio of the combustion heating energy to the initial thermal energy of the flow, and is sometimes used in combustion theory.

$$\dot{m}_F \left( \frac{HV}{c_p T_{Amb}} \right) = \dot{m}_A T^* \quad (9)$$

$$HV^* \equiv \frac{HV}{c_p T_{Amb}} \quad (10)$$

Substituting the dimensionless mass air flow rate defined in Eq. (6), into Eq. (9), yields Eq. (11). A dimensionless fuel mass flow rate, of a similar form to the dimensionless air flow rate of Eq. (6) can be defined as shown in Eq. (12).

$$\dot{m}_F HV^* = \dot{m}_A^* CA\rho_{Amb}\sqrt{ghT^*} \quad (11)$$

$$\dot{m}_F^* \equiv \frac{\dot{m}_F}{CA\rho_{Amb}\sqrt{gh}} \quad (12)$$

Using the dimensionless mass fuel flow rate  $\dot{m}_F^*$ , the final form of the dimensionless heat addition equation becomes that of Eq. (13).

$$\dot{m}_F^* HV^* = \dot{m}_A^* T^* \quad (13)$$

### Air/fuel ratio from the dimensionless model

The air/fuel ratio (AFR) can be conveniently recognized by rearranging Eq. (13) as shown in Eq. (14).  $HV^*$  will remain constant for stove operation, and it is interesting to note a simple inverse linear relationship between  $T^*$  and the AFR.

$$AFR \equiv \frac{\dot{m}_A}{\dot{m}_F} = \frac{HV^*}{T^*} \quad (14)$$

The equivalence ratio ( $\Phi$ ) will be used for plotting, and is related to the AFR as defined in Eq. (15), where  $AFR_{stoich}$  is the air/fuel ratio for a stoichiometric mixture. Excess air ratio (EAR) is another method for describing the AFR. EAR was used instead of AFR throughout Agenbrood et al. (2011), and will be used again briefly in Carbon monoxide emissions. EAR is defined as shown in Eq. (16).

$$\Phi = \frac{AFR_{stoich}}{AFR} \tag{15}$$

$$\%EAR = \frac{(1-\Phi) \cdot 100\%}{\Phi} \tag{16}$$

*Dimensionless system results*

Eqs. (7) and (11) together define the dimensionless simplified stove flow model analogous to the dimensional results of Agenbrood et al. (2011). Stove geometry no longer appears directly in either equation and enters only through the definition of the dimensionless air and fuel mass flow rates. As noted in Agenbrood et al. (2011) for the dimensional case, geometry parameters appear only together as the product of  $CA\sqrt{h}$ . This  $CA\sqrt{h}$  product essentially scales the dimensional mass air flow rate and firepower to scale similarity in the dimensionless form for use in Eqs. (7) and (11).

Eqs. (7) and (11) can be used iteratively in the same manner as the dimensional system. The resulting dimensionless stove behavior plot is shown in Fig. 1.

The shape and qualitative behavior of the curves shown in Fig. 1 are the same as the dimensional model results of Agenbrood et al. (2011). The x-axis product,  $\dot{m}_F^* HV^*$ , is analogous to the firepower x-axis used in Agenbrood et al. (2011).  $\dot{m}_F^*$  and  $T^*$  are of course analogous to the dimensional  $\dot{m}_F$  and  $T_H$ , and again behave in a similar manner, only scaled.

Fig. 1 can be used to lookup solutions for a given stove geometry and firepower of interest without solving the model system. The firepower is first converted to a dimensionless form using Eqs. (11) and (10) and the geometry of interest. Fig. 1 is then used to lookup the corresponding dimensionless mass air flow and temperature. These values are then returned to their dimensional form using Eqs. (3) and (6) for practical dimensional use. Air and fuel mass flow rate can be determined using Fig. 1 in a manner. For a desired AFR, the corresponding  $T^*$  can be easily calculated from Eq. (14).

**With cook piece validation**

Part 1, Agenbrood et al. (2011), validation was for somewhat an idealized case of a stove operating without a cook piece in place. As noted, this configuration was useful for isolating the basic model physics and assessing model accuracy while minimizing the effect of

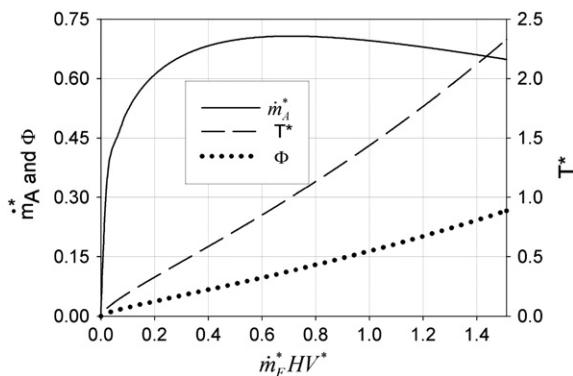


Fig. 1. Non-dimensional mass flow rate, temperature, and equivalence ratio behavior. This plot can also be used to lookup dimensionless solutions for conversion to dimensional use.

the unknown loss coefficient and neglected heat transfer. Validation is now extended to stove operation with the cook piece in place to examine model application to more practical cooking use.

Bulk mass flow rate and temperature is measured for comparison to model predicted behavior, as well as the related emissions (not directly predicted by the model), analogous to Agenbrood et al. (2011). The with cook piece configuration emission results are shown to be significantly more interesting than the without cook piece configuration, particularly with the help of the dimensionless form developed in Development of the dimensionless system.

*Experimental setup*

Experimental setup and procedure is similar to the without cook piece validation of Agenbrood et al. (2011), and should be considered unchanged unless noted otherwise. The fiberfrax insulated 4 in rocket elbow stove is used once again; Agenbrood et al.'s (2011) without cook piece data is included for comparison. The stove has been fitted with an Envirofit model G3300 (<http://www.envirofit.org/>) drip pan as shown in Fig. 2. The G3300 drip pan has built in supports for locating the cook piece resulting in an 18 mm pot gap at the narrowest point. A stainless steel cook piece of 225 mm diameter containing 5 l of boiling water is used. Cook piece water temperature affects the heat transfer rate (with a higher  $\Delta T$  producing higher rates), therefore the water temperature must remain consistent between tests. Boiling water is simple to maintain and monitor; cook piece water is raised to a boiling temperature before sampling data.

As in Agenbrood et al. (2011) the stove is burned by hand, insuring practical application, but requiring temporal averaging of the results. Two “test sweeps” are performed with the cook piece in place. As in Agenbrood et al. (2011), a “test sweep” consists of five 15 minute data sampling periods over which firepower is held, by an experienced operator, as constant as possible. The five sampling periods are at varying target firepowers, with 15 minute transient periods in between sampling to allow the stove to adjust to the new firepower level and reach an approximately steady state behavior. Temporal averaging is then applied to the 15 minute data samples yielding the values used for validation. An attempt is made to hit the firepower points of the previous 4 in rocket elbow validation data of Agenbrood et al. (2011).

Mass based CO and CO<sub>2</sub> emissions are used to calculate the current firepower of the stove using a simple carbon balance. Knowing the

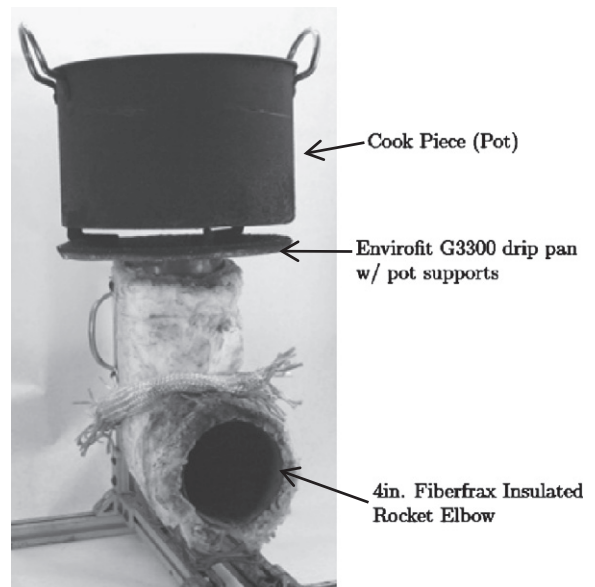


Fig. 2. Rocket elbow stove with cook piece validation setup.

firepower, the exhaust stack  $\%O_2$  can be used to measure mass flow rate. The method for determining both firepower and mass flow rate has been described in Agenbrood et al. (2011) and can be referenced for a more detailed description. Due to interference with the cook piece,  $\%O_2$  sampling and thermocouple location must be slightly lower than the previous work. The modified location is approximately in the middle of the cook piece drip pan gap and about 10 mm lower than without the cook piece in place.

#### Dimensional results and discussion

With cook piece validation results are first examined using the dimensional form for direct comparison with the dimensional results of Agenbrood et al. (2011) and to contrast the benefits of the dimensionless form to be presented in Dimensionless results.

#### Bulk flow rate

With cook piece validation results from the temporally averaged 15 minute data samples of  $\%O_2$ , mass air flow rate, and temperature are shown in Fig. 3. Corresponding without cook piece 4 in rocket elbow validation data from Agenbrood et al. (2011) is shown for comparison in a lighter shade. Model predicted behavior for a range of three loss coefficient values is also shown.

Model predicted trends remain in agreement with both the model predicted behavior and the without cook piece results, but at consistently lower flow rates and higher temperatures. This behavior can be explained by the likely increase in viscous losses due to the cook piece flow restriction. In Agenbrood et al. (2011), model predicted behavior using a loss coefficient of 0.5 was shown to agree well with the without cook piece validation data. Ideal flow behavior with a loss coefficient equal to 1 was also shown for reference. In addition to those used in the previous work, a third line is produced using an experimentally determined loss coefficient of 0.35. Accounting for the additional cook piece restriction, model predicted behavior for this loss coefficient agrees well with the new data. This additional loss is higher than initially expected, and burning the stove at firepowers corresponding to the without cook piece validation was not possible for some higher powers. The highest firepower achieved in either test run was around 4 kW.

#### High firepower outliers

Two high firepower outliers are observed in the with cook piece validation data of Fig. 3. One likely explanation is as follows:

As proposed in Agenbrood et al. (2011), exhaust  $\%O_2$  and bulk excess air ratio can relate an operating firepower to a stove configuration's firepower range, in particular, relative to a stove's upper firepower limit. For the high firepower outliers, measured  $\%O_2$  is around 2%, and with the 0.35 loss coefficient model predicted excess air ratio is around 40%. These values are much lower than those reached in the previous work validation data (for all but the failed high firepower attempts), and suggest a very high firepower relative to the current stove configuration.

Considering the poor mixing inherent to biomass cook stoves of this type, combustion in this region is likely oxygen starved. In this case, unburned volatiles would continue to decrease  $\%O_2$ , but without the increase in firepower that would have resulted from their combustion. This explanation is consistent with the observed behavior of the high firepower outliers.

#### Bulk flow temperature

With the 0.35 loss coefficient, model predictions agree well with the measured  $\%O_2$  and mass flow rate validation results. Consistent with Agenbrood et al. (2011), validation measured flow temperatures, shown in Fig. 3, are lower than predicted by the model, and are again likely explained by inaccuracies of the adiabatic assumption.

As predicted by the model using the 0.35 loss coefficient, with cook piece validation temperature results are observed to be higher than

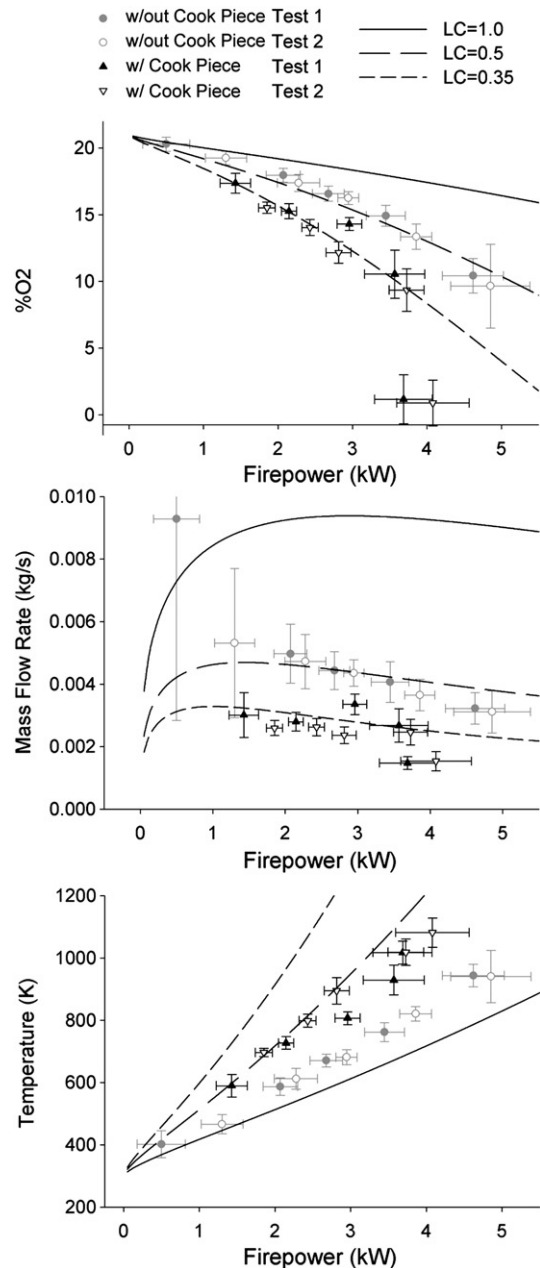


Fig. 3. Rocket elbow with cook piece validation results with comparison to Agenbrood et al. (2011) without cook piece results (shown in lighter shade) and model predicted behavior.

those without the cook. This temperature increase is competing with an effect not addressed in the model—an expected increase in air flow heat loss to the relatively cold and high thermal mass cook piece. With the observed temperature increase, the decrease in thermal mass is observed to be more significant than the increase in flow heat loss.

#### Carbon monoxide emissions

As in Agenbrood et al. (2011), CO emissions will be described using the modified combustion efficiency (MCE). MCE is defined in Eq. (17).

$$MCE = \frac{CO_2}{CO + CO_2} \quad (17)$$

With cook piece MCE data are shown in Fig. 4 with comparison to Agenbrood et al.'s (2011) without cook piece data (in a lighter shade)

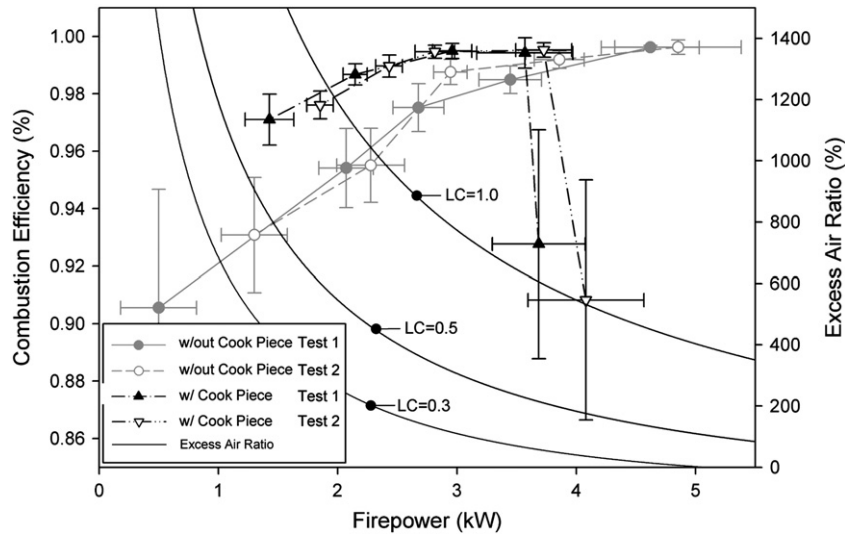


Fig. 4. Rocket elbow with cook piece CO emission results (plotted as MCE) with comparison to Agenbrood et al. (2011) without cook piece results (shown in lighter shade) and model predicted excess air ratio.

and model predicted EAR. At low firepower, an increase in MCE is observed once again with increasing firepower. This behavior is consistent with the without cook piece results from the previous work, although shifted towards lower firepowers. In Agenbrood et al. (2011), this increasing MCE was suggested to result from the decreasing, large, EAR. Considering the model predicted EAR behavior for the 0.35 (with cook piece) and 0.5 (without cook piece) loss coefficient, with cook piece behavior is essentially shifted to the right relative to the without cook piece results. After shifting, the MCE–EAR behavior of the two curves looks to be in agreement. In the following section, application of the dimensionless form to these results will provide further insight into this effect.

At high firepower, MCE data corresponding to the previously discussed outliers behave in a particularly interesting manner. With these points a sharp reduction in combustion efficiency is observed, suggesting an upper, high firepower, low EAR, efficient combustion limit. This high firepower reduction appears much steeper here than the onset of good combustion with increasing low firepower.

This high firepower, low EAR, efficient combustion limit was proposed In Agenbrood et al. (2011). An attempt was made to reach and observe this limit, but the behavior of interest was not observed. Instead, as the chimney region became oxidizer starved, it was suggested that combustion was able to proceed with entrainment air after exiting the chimney, and no significant detriment to combustion efficiency was observed. In the present work, with a cook piece now in place, it appears that this is no longer the case. The exact mechanism, or combination thereof, responsible for this behavior is uncertain. The following observations may be of significance: first, entrainment air can no longer be reached immediately at the top of the chimney flow. Second, the flame aerodynamic disturbance of the cook piece may be important. Third, it is also possible that the pot removes enough heat from the flow that combustion can no longer proceed in an efficient manner after leaving the chimney and reaching entrainment air.

Particulate matter emissions

Particulate matter emission data will be plotted using the emission factor as defined in Eq. (18).

$$EF = \frac{\text{g of Particulate Matter}}{\text{kg of Fuel Burned}} \tag{18}$$

With cook piece EF data are shown in Fig. 5. Without cook piece results from Agenbrood et al. (2011) are again shown in a lighter shade.

Prior to experimentation, the effect of having the cook piece in place on particulate matter emissions would be difficult to predict; two major and competing effects were considered: first, buildup of particulate matter on the cook piece due to impaction is known to occur, thus removing particulate matter before reaching the filter for gravimetric analysis. Second, radiative quenching of particles (after formation, but before passing through the flame sheet) is often thought to affect the likelihood of a particle’s oxidation. The relatively cool and immediate cook piece will likely encourage radiative heat exchange from particulate matter, reducing the likelihood of oxidation and increasing the EF.

From the data in Fig. 5, a steep increase in EF is observed at higher firepowers. The low firepower EF increase observed without the cook piece in Agenbrood et al. (2011) is not observed clearly here. Considering the with/without cook piece shifted behavior suggested in the previous section, low enough firepower sampling may not have been taken to observe a low firepower EF increase. The opposite may be true for the Agenbrood et al. (2011) without pot results and the high firepower EF increase—although it is also possible that the steep particulate matter increase may only occur with a cook piece in place, as observed with CO modified combustion efficiency. The dimensionless form will provide insight into the shifted data here as well, and will be applied in the following section.

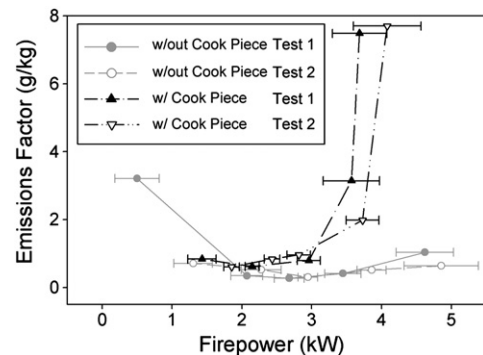


Fig. 5. Rocket elbow with cook piece PM emission results (plotted as EF) with comparison to Agenbrood et al. (2011) without cook piece results (shown in lighter shade).

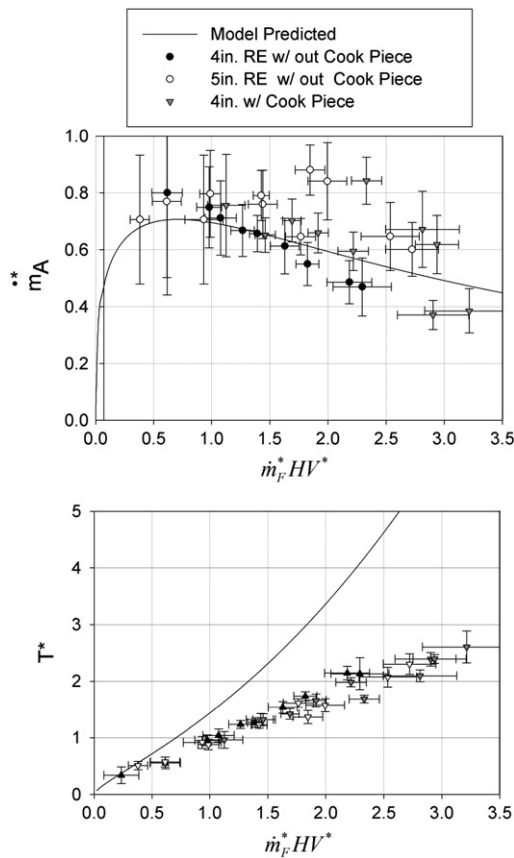


Fig. 6. Dimensionless mass flow rate and temperature results for the three stove configurations—from this and the previous work, Agenbroad et al. (2011)—plotted together for direct comparison with a single trend for each parameter.

**Dimensionless results**

*Bulk flow rate and temperature*

As discussed in Development of the dimensionless system, with the dimensionless form, plots analogous to Agenbroad et al.'s (2011) Fig. 6 no longer exist; stove behavior will now be independent of stove geometry

and validation data from varying stove geometries and configuration can be plotted together directly to form single bulk flow rate and temperature trends. Validation data for both Agenbroad et al. (2011) geometries (4 in and 5 in diameter rocket elbow without cook piece) as well as the with cook piece results from Dimensional results and discussion are shown plotted together in Fig. 6. The dimensionless model predicted stove behavior from Development of the dimensionless system is shown for comparison.

The validation data fits well and now follows a single mass flow rate and temperature trend line for the three stove configurations. Once again experimental temperature data falls significantly below the predicted values, likely for the reasons already discussed with regards to the dimensional results.

*Emissions*

The dimensionless form will also be applied to the emission data; with this application, its utility will be particularly apparent. MCE and EF data taken for the three stove configurations are plotted using a dimensionless firepower axis ( $m_F HV$ ) in Fig. 7.

Using the dimensionless firepower, the with and without cook piece results contribute to a single trend for both PM and CO emissions. The shifted data noted in the dimensional form with regards to Figs. 3–5 has been accounted for with the dimensionless axis. Both CO and PM emission trends are observed and appear to trend together. This is a convenient result for the stove designer, allowing both criteria to be satisfied simultaneously. An efficient combustion region is observed at dimensionless firepowers between approximately 1.5 and 2.5. This region has also been labeled in Fig. 7. Both carbon monoxide and particulate matter emissions are significantly improved within this region and begin to deteriorate outside of it. With only three stove configurations, two “test sweeps” each, these findings should likely be considered preliminary, but they do suggest a design tool with a great deal of potential and warranting future exploration.

If a stove where to be designed for a desired operating firepower, a stove geometry could be determined that would place the firepower with the efficient combustion dimensionless firepower range. The stove designer may not have reliable control over the firepower that a stove will be operated at during actual use in the field. In this case, if the typical field operating firepower can be determined, it may be possible to tune the stove into this efficient combustion region. For example, if the stove tends to be operated in the field at firepowers above the dimensionless

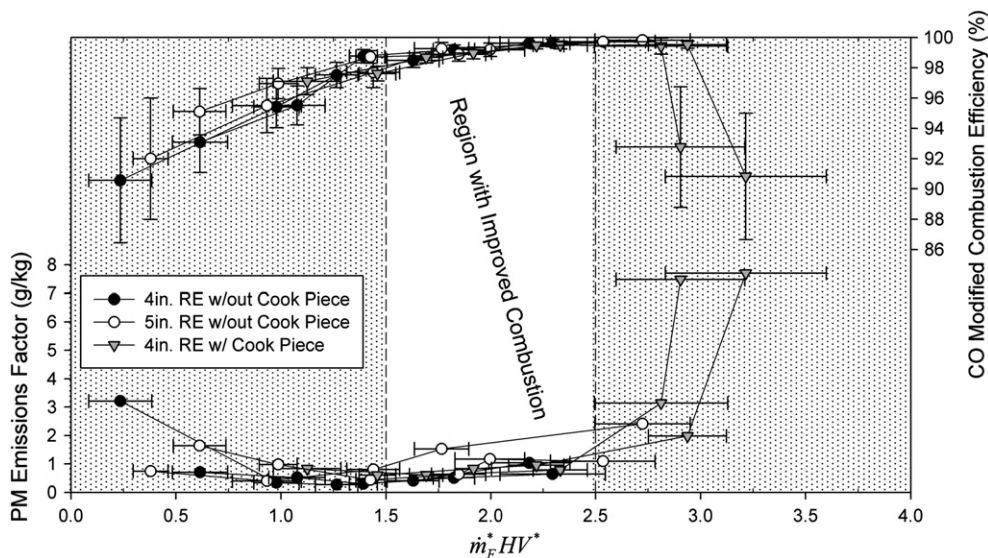


Fig. 7. Dimensionless CO and PM emission results (plotted as MCE and EF respectively) for the three stove configurations. With the dimensionless firepower axis, emission data can be combined into a single trend for each criteria, and an improved combustion region is observed for the dimensionless firepower range shown.

efficient combustion range, the stove designer might reduce the loss coefficient to shift the dimensionless range for the stove toward the firepower being observed in the field (assuming this firepower could remain sufficiently constant while the design is modified).

## Conclusions

The simple model presented in the preceding work of Part 1, Agenbroad et al. (2011) has herein been further developed into a dimensionless form; this form has shown several advantages including a general solution that is independent of specific stove geometry and a reduction of independent experimental parameters.

The dimensionless form was applied to the two configurations of the preceding work as well as a third “with cook piece” validation configuration included in this work. This with cook piece configuration has extended the previous, somewhat idealized validation performed without a cook piece to more practical operation, verifying model application and accuracy for more practical cooking use. Validation with the cook piece has also allowed an upper limit to firepower and efficient combustion to be observed.

Using the dimensionless form, the three validation configuration results are plotted together independent of geometry, allowing direct comparison and showing consistency and agreement between all validation data and the simplified stove flow model. Plotting with the dimensionless form, the three configurations create single mass flow rate and temperature trends.

Applying the dimensionless form to the *CO* and *PM* emission data taken with validation provides a particularly useful reduction of independent experimental parameters; emission data from the three configurations form single trends for both *CO* and *PM*. The two criteria trend together and an efficient combustion region was observed over a range of medium dimensionless firepowers. If stoves could be designed such that operation would be in this region, harmful emissions could likely be reduced.

### Future work

Experimental validation has been consistent and demonstrated model utility for the three configurations examined thus far. However, with only three configurations, more experimentation is likely necessary to understand the extent, accuracy, and consistency of the model application for direct model predictions such as bulk mass flow rate and temperature and empirically determined emission trends.

Although it appears that *CO* and *PM* emissions are improved in the improved emission region, the direct mechanism is unknown and more understanding would be both interesting and useful. It has been proposed, particularly in Agenbroad et al. (2011) that EAR is important to *CO* MCE as quenching is reduced and as sufficient oxygen is supplied. Particulate matter formation and destruction is likely an even more elusive emission phenomena. Many complex and competing factors such as particle radiative heat transfer, competition for OH radicals, flame length and thickness are thought to be important. Frenklach (2002), Roper (1984) and Kent and Wagner (1984) have been especially thought provoking.

Applying the model presented here to predicting heat transfer is a particularly interesting possibility. The bulk temperature and mass flow rate outputs of the model are useful as fundamental inputs for CFD heat transfer studies. Viskanta (1993) provides a good review of impingement heat transfer (similar to the stove pot interface) for

cases with and without combustion. A theoretical description and several solutions and correlations are presented. Relatively little work has been performed at sufficiently slow (low Reynolds number) flow and small nozzle to plate distances for ready application to biomass cooking stoves. Spalart and Allmaras (1989) is useful and nearly applicable for the rocket elbow case discussed here. In any case (CFD or correlation), the reacting flow and stove/pot interface feedback to the fire are two particularly important and complicating issues.

Both heat transfer and particulate matter predictions may benefit from predicting flame length. Non-premixed flame lengths for enclosed laminar diffusion flames, with similar inputs as those provided by the model here, have been predicted with significant assumptions (steady, 1-D flow, etc.) by Roper (1977) and Roper et al. (1977), although much higher flow rates and unsteady behavior must be considered to extend this work to biomass cook stoves applications. The unsteady flame shape might be studied numerically (CFD) with unknown accuracy using a probability density function mixture fraction and a Large Eddy Simulation turbulence model.

Future work also exists in determining, understanding, and controlling the loss coefficient. Constant values of 0.35, 0.5, and 1 have been used with relative success thus far. This loss coefficient is likely an important tool/parameter in stove design. A non-constant loss coefficient might depend on model variables such as flow rate and temperature.

Finally, with the development of the above envisioned heat transfer and emission extensions, the use of automated optimization algorithms may be possible to search for target performance goals, determining the best stove configuration for a given application.

## Acknowledgements

This work has been supported by the Colorado State University Engines and Energy Conversion Laboratory with funding from Envirofit International and the Shell Foundation's Breathing Space Program. Special thanks to Melanie Sloan, Christian L'Orange, Dan Lionberg, and Dr. Anthony Marchese—for your help, expertise, and advice, but also for a great experience in general.

## References

- Agenbroad J, DeFoort M, Kirkpatrick A, Kreutzer A. A simplified model for understanding natural convection biomass cooking stoves—Part 1: Setup and baseline validation. *Energy for Sustainable Development* 2011;15(2):169–75.
- Frenklach M. Reaction mechanism of soot formation in flames. *Phys Chem Chem Phys* 2002;4:20282037 URL [http://www.rsc.org/delivery/\\_ArticleLinking/DisplayArticleForFree.cfm?doi=b110045a&JournalCode=CP](http://www.rsc.org/delivery/_ArticleLinking/DisplayArticleForFree.cfm?doi=b110045a&JournalCode=CP) February.
- Kent J, Wagner H. Why do diffusion flames emit smoke. *Combustion Sci Technol* 1984;41(5–6):245–69 november.
- Roper F. The prediction of laminar jet diffusion flame sizes: part I. Theoretical model. *Combustion Flame* 1977;29:219–26 URL <http://www.sciencedirect.com/science/article/B6V2B-497SDH9-9N/2/6ecb89dc540fa391994deb2929d716f>.
- Roper F, Smith C, Cunningham A. The prediction of laminar jet diffusion flame sizes: part II. Experimental verification. *Combustion Flame* 1977;29:227–34 URL <http://www.sciencedirect.com/science/article/B6V2B-497SDH9-9P/2/68e242eefcf4d51262f20387d81ebe50>.
- Roper FG. Soot escape from diffusion flames: a comparison of recent work in this field. *Combustion Sci Technol* 1984;40(5–6):323–9 URL <http://www.informaworld.com/smpp/content-db=all-content=a778731127-tab=citation>.
- Spalart PR, Allmaras SF. Heat transfer in confined laminar axisymmetric impinging jets at small nozzle-plate distances: the role of upstream vorticity diffusion. *Num Heat Transf A Appl* 1989;39(8):777–800 URL <http://www.informaworld.com/smpp/content-content=a713837278&db=all>.
- Viskanta R. Heat transfer to impinging isothermal gas and flame jets. *Exp Therm Fluid Sci* 1993;6(2):111–34 URL <http://www.sciencedirect.com/science/article/B6V34-48188SJ-1G/2/eb0a2de08e4c65c3b9ce2e340c73c30a>.